Biochimica et Biophysica Acta 1777 (2008) 1109–1115

Contents lists available at ScienceDirect

Biochimica et Biophysica Acta

journal homepage: www.elsevier.com/locate/bbabio

# Acceptor side effects on the electron transfer at cryogenic temperatures in intact photosystem II

Han Bao [a], Chunxi Zhang [a,*], Keisuke Kawakami [b], Yanan Ren [a], Jian-Ren Shen [b], Jingquan Zhao [a]

[a] Laboratory of Photochemistry, Beijing National Laboratory of Molecular Sciences, Institute of Chemistry, Chinese Academy of Sciences, Beijing 100080, China
[b] Graduate School of Natural Science and Technology/Department of Biology, Faculty of Science, Okayama University, Tsushima-naka, Okayama 700-8530, Japan

ARTICLE INFO

*Article history:*
Received 17 October 2007
Received in revised form 16 April 2008
Accepted 16 April 2008
Available online 9 May 2008

*Keywords:*
Photosystem II
TyrZ
Side-path electron donor
Non-heme iron
EPR
Electron transfer

ABSTRACT

In intact PSII, both the secondary electron donor ($Tyr_Z$) and side-path electron donors ($Car/Chl_Z/Cyt_{b559}$) can be oxidized by $P_{680}^{+\cdot}$ at cryogenic temperatures. In this paper, the effects of acceptor side, especially the redox state of the non-heme iron, on the donor side electron transfer induced by visible light at cryogenic temperatures were studied by EPR spectroscopy. We found that the formation and decay of the $S_1Tyr_Z\cdot$ EPR signal were independent of the treatment of $K_3Fe(CN)_6$, whereas formation and decay of the $Car^{+\cdot}/Chl_Z^{+\cdot}$ EPR signal correlated with the reduction and recovery of the $Fe^{3+}$ EPR signal of the non-heme iron in $K_3Fe(CN)_6$ pre-treated PSII, respectively. Based on the observed correlation between $Car/Chl_Z$ oxidation and $Fe^{3+}$ reduction, the oxidation of non-heme iron by $K_3Fe(CN)_6$ at 0 °C was quantified, which showed that around 50–60% fractions of the reaction centers gave rise to the $Fe^{3+}$ EPR signal. In addition, we found that the presence of phenyl-*p*-benzoquinone significantly enhanced the yield of $Tyr_Z$ oxidation. These results indicate that the electron transfer at the donor side can be significantly modified by changes at the acceptor side, and indicate that two types of reaction centers are present in intact PSII, namely, one contains unoxidizable non-heme iron and another one contains oxidizable non-heme iron. $Tyr_Z$ oxidation and side-path reaction occur separately in these two types of reaction centers, instead of competition with each other in the same reaction centers. In addition, our results show that the non-heme iron has different properties in active and inactive PSII. The oxidation of non-heme iron by $K_3Fe(CN)_6$ takes place only in inactive PSII, which implies that the $Fe^{3+}$ state is probably not the intermediate species for the turnover of quinone reduction.



## 1. Introduction

PSII is a multi-subunit membrane protein complex that catalyzes the oxidation of water to oxygen and the reduction of plastoquinone to plastoquinol using sun light. Its structure has been reported by several groups at resolutions from 3.8 to 3.0 Å [1–5]. The arrangement of PSII reaction center cofactors involved in electron transfer is shown in Fig. 1.

Upon excitation at physiological temperatures, the primary electron donor ($P_{680}$) donates one electron to the primary electron acceptor (Pheo), producing the $P_{680}^{+\cdot}$ and $Pheo^{-\cdot}$ charge pair [6–9]. $Pheo^{-\cdot}$ transfers the electron to the primary and secondary quinone acceptors ($Q_A$ and $Q_B$) in sequence at the acceptor side. $Q_B$ becomes fully reduced after two turnovers of the primary reaction, which is then exchanged with oxidized plastoquinone from the PQ pool in thylakoid membranes. There is a non-heme iron between $Q_A$ and $Q_B$, which may play roles in regulating the electron transfer between them [10,11].

Meanwhile, $P_{680}^{+\cdot}$ is reduced by the secondary electron donor $Tyr_Z$ in tens of ns, resulting in a neutral radical, $Tyr_Z\cdot$. $Tyr_Z\cdot$ then drives the water oxidation in the catalytic center of the Mn-cluster containing four Mn ions, one $Ca^{2+}$ and one or more $Cl^-$ ions. The turnover of the Mn-cluster leading to water oxidation involves five different states ($S_n$, n= 0, 1, 2, 3, 4), in which $S_0$ is the most reduced state, and $S_1$ is the dark stable state (see reviews [12–17]). Although $Tyr_Z$ plays an important role in tuning the photochemical reaction and the catalytic water oxidation process, studies on $Tyr_Z\cdot$ in intact PSII have been limited because of its fast turnover and lack of spectroscopic characteristics at physiological conditions [18–20]. The detailed mechanism of catalytic reaction involving $Tyr_Z$ is still waiting for a clear answer, although various models have been proposed [21–28].

$P_{680}^{+\cdot}$ can also oxidize some accessory cofactors called side-path electron donors [29–31], which includes two Chla molecules ($ChlZ_{D1}$, $ChlZ_{D2}$), two Car molecules ($Car_{D1}$ and $Car_{D2}$) and one $Cyt_{b559}$, as shown in Fig. 1. Although these components constitute a significant

*Abbreviations:* Chl, chlorophyll; $Chl_Z$, side-path redox active Chl; Car, redox active β-carotene; $Cyt_{b559}$, cytochrome *b*559; D1, D2, reaction center core proteins; DMSO, dimethyl sulfoxide; EDTA, ethylenediaminetetraacetic acid; EPR, electron paramagnetic resonance; LBHB, low-barrier hydrogen bond; MES, 4-morpholine ethanesulfonic acid; $P_{680}$, primary electron donor of PSII; $P_{D1}$, $P_{D2}$, two monomeric Chls of $P_{680}$ associated with $D_1$ and $D_2$, respectively; Pheo, pheophytin; PPBQ, phenyl-*p*-benzoquinone; PSII, photosystem II; $Q_A$ and $Q_B$, primary and secondary quinone electron acceptors, respectively; $Tyr_Z$, tyrosine 161 of the $D_1$ protein; $Tyr_D$, tyrosine 160 of the $D_2$ protein

* Corresponding author. Tel.: +86 10 82617053; fax: +86 10 82617315.
*E-mail address:* chunxizhang@iccas.ac.cn (C. Zhang).

0005-2728/$ – see front matter © 2008 Elsevier B.V. All rights reserved.
doi:10.1016/j.bbabio.2008.04.044

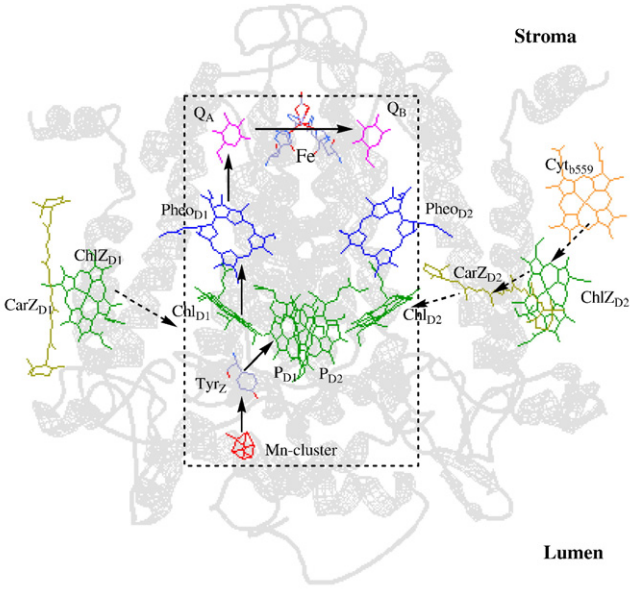


**Fig. 1.** Arrangement of PSII reaction center cofactors. The Mn-cluster, Chla, Pheo, quinone, Car and $Cyt_{b559}$ are shown in red, green, blue, purple, yellow, orange, respectively. For clarity, the tails of Chla, Pheo, $Q_A$ and $Q_B$ molecules are omitted. Solid and dashed arrows indicate the main and side-pathways of electron transfer, respectively.

proportion of the cofactors in PSII reaction center, their functions in intact PSII are still under debate [29,30]. It was generally suggested that they play roles in protecting the PSII reaction center from photo-inhibition and photo-damage; however, studies on these side-path electron donors are hampered by their slow electron donation rate to $P_{680}^{+\cdot}$ and extremely low quantum yield at physiological conditions [30].

At cryogenic temperatures, although the water oxidation and $Q_B$ reduction processes are blocked [32,33], primary charge separation and most of the secondary electron transfer reactions are still accessible. The oxidation of side-path electron donors at cryogenic temperatures has been reported for many years [29,30,34–40], whereas, it was considered that $Tyr_Z$ could not be oxidized at cryogenic temperatures. This opinion has been changed recently by reports on a relatively high yield (40–50%) of $Tyr_Z$ oxidation in intact PSII samples induced by visible light illumination at cryogenic temperatures [41–44]. The magnetic interaction between $Tyr_Z\cdot$ and $S_0$ or $S_1$ states of the Mn-cluster gives rise to two distinctive EPR signals attributed to $S_0Tyr_Z\cdot$ and $S_1Tyr_Z\cdot$, respectively. At cryogenic temperatures the life-times of $Car^{+\cdot}/Chl_Z^{+\cdot}$ and $Tyr_Z\cdot$ are known to be hours and a few minutes, respectively, which are much longer than those at physiological temperatures. Accordingly, the investigation of the low temperature electron transfer processes in intact PSII may shed new light on the function and mechanism of $Tyr_Z$, as well as the side-path electron donors.

It is known that the change of the donor side could significantly affect the electron transfer at the donor side in PSII (see ref. [45–48] for example). In this paper, we have investigated the effect of acceptor side on the electron transfer in intact PSII at cryogenic temperatures with the method developed recently [42,44]. We have found that the oxidizability of the non-heme iron by $K_3Fe(CN)_6$ and the presence of oxidized quinone molecule at $Q_B$ position significantly affect the type of the electron transfer occurred at the donor side. Our results suggest that the oxidation of $Tyr_Z$ and the side-path donors may occur separately in different PSII reaction centers, and the non-heme $Fe^{3+}$ is probably not the intermediate species during the turnover of $Q_B$ reduction.

## 2. Materials and methods

PSII enriched membranes were isolated from spinach as in Ref. [49] with some modifications. Fresh spinach leaves were ground in a buffer containing 400 mM Sucrose, 400 mM NaCl, 5 mM $MgCl_2$, 1 mM EDTA, 5 mM ascorbic acid, 1.7 g/l BSA, 25 mM HEPES/NaOH, (pH 7.5). The pelleted chloroplasts were washed with a buffer containing 100 mM NaCl, 8 mM $MgCl_2$, 25 mM MES-NaOH (pH 6.0), then resuspended in a buffer containing 15 mM NaCl, 10 mM $MgCl_2$, 25 mM MES-NaOH (pH 6.0) and treated with 25 mg of Triton X-100/mg of Chl at a concentration of 2 mg of Chl/ml for 30 min. The PSII membranes were subsequently washed with buffer containing 400 mM Sucrose, 15 mM NaCl, 5 mM $MgCl_2$, 5 mM $CaCl_2$, 25 mM MES-NaOH, (pH 6.5). All procedures were carried out on ice or 0 °C under dim green light or darkness. The final PSII membranes were frozen into liquid nitrogen and stored at −80 °C until use. Typical oxygen evolving rate was 600–800 μmol $O_2$ (mg Chl)$^{-1}$ h$^{-1}$, measured with a Clark-type electrode at 25 °C in the presence of 0.3 mM PPBQ.

EPR samples from spinach were prepared as following. PSII enriched membranes were thawed and washed with a buffer containing 400 mM sucrose, 15 mM NaCl, 5 mM $CaCl_2$, 1 mM EDTA, and 25 mM MES/NaOH pH 6.5. The pellet was dissolved into the same buffer to a Chl concentration of 1 mg/ml, then exposed to room-light at 0 °C for 2 min to synchronize all reaction centers to the $Tyr_D^{\cdot}S_1$ state. The samples were washed once more, resuspended in the same buffer without EDTA, and then filled into EPR tubes. After two to three hours dark adaptation at 0 °C, PPBQ from a fresh 20 mM solution in DMSO was added to a final concentration of 1 mM as an external electron acceptor. After addition of PPBQ, the sample was frozen, first in dry ice/ethanol, then in liquid nitrogen. EPR samples without PPBQ were prepared in the same way by adding DMSO only. Final Chl concentration of the EPR samples was 10–12 mg Chl/ml.

$K_3Fe(CN)_6$ treatment of PSII enriched membranes was performed as described in ref. [50]. Samples were incubated with 10 mM $K_3Fe(CN)_6$ from a freshly prepared solution on ice for 60 min in the dark, then PPBQ in DMSO was added to a final concentration of 1 mM. Then the samples were frozen in EPR tube, first in dry ice/ethanol, then in liquid nitrogen.

PSII core complexes from *Thermosynechococcus vulcanus* (*T. vulcanus*) were purified as described in Ref. [51] and filled into EPR tubes. $K_3Fe(CN)_6$ treatment was performed with the same procedures for spinach PSII membranes as described above.

Low temperature continuous wave EPR spectra and kinetics were recorded on a Bruker E500 spectrometer equipped with an Oxford ESR 900 liquid helium cryostat and ITC-503 temperature controller. A super-high sensitive resonance cavity with an optical window was used for all of the measurements. Before EPR measurements, all samples were degassed with nitrogen gas at 200 K. Continuous visible light illumination at liquid helium temperature was carried out directly in the EPR cavity as described in ref [44,52]. Most EPR spectra were measured in low microwave power (1 mW) in order to avoid signal saturation which made the evaluation and quantification of the $S_1Tyr_Z\cdot$ signal more difficult. EPR spectra of $Car^{+\cdot}/Chl_Z^{+\cdot}$ were recorded with microwave power of 1 μW. Other spectrometer settings are given in the figure legends.

## 3. Results

Previous studies have demonstrated that $Tyr_Z$ oxidation at cryogenic temperatures is strongly dependent on the integrity and S-states of the Mn-cluster [42,44]. To investigate the acceptor side effects on the electron transfer in PSII reaction center at cryogenic temperatures, the Mn-cluster is kept intact and in $S_1$ state in all of the experiments.

In our experiments, we have modified two components at the acceptor side. One is the non-heme iron, which is coordinated by four His residues provided by D1 and D2 proteins and one non-protein ligand (bicarbonate/carbonate). The other is the $Q_B$ molecule, which can be readily removed from its binding site or replaced by other quinone molecules.

### 3.1. Non-heme iron effect

Generally, the non-heme iron is in the $Fe^{2+}$ state, and can be oxidized to $Fe^{3+}$ by external oxidants [50,53,54]. It has been well documented that non-heme iron in PSII can be oxidized by $K_3Fe(CN)_6$ at 0 °C [54]. The oxidized non-heme iron, $Fe^{3+}$, has a distinguished EPR signal at $g$=8.0–5.0 range [50,53,54]. The $Fe^{3+}$ ion can be reduced by $Q_A^{-\cdot}$ rapidly [54], which occurs even at cryogenic temperatures [53–55]. From the previous reports [42, 44], we know that when the non-heme iron is in the $Fe^{2+}$ state, the $S_1Tyr_Z\cdot$ EPR signal ($g$=2.03) decays in the dark with a life-time of about 5 min due to the charge recombination between $Q_A^{-\cdot}$ and $S_1Tyr_Z\cdot$. One would anticipate a

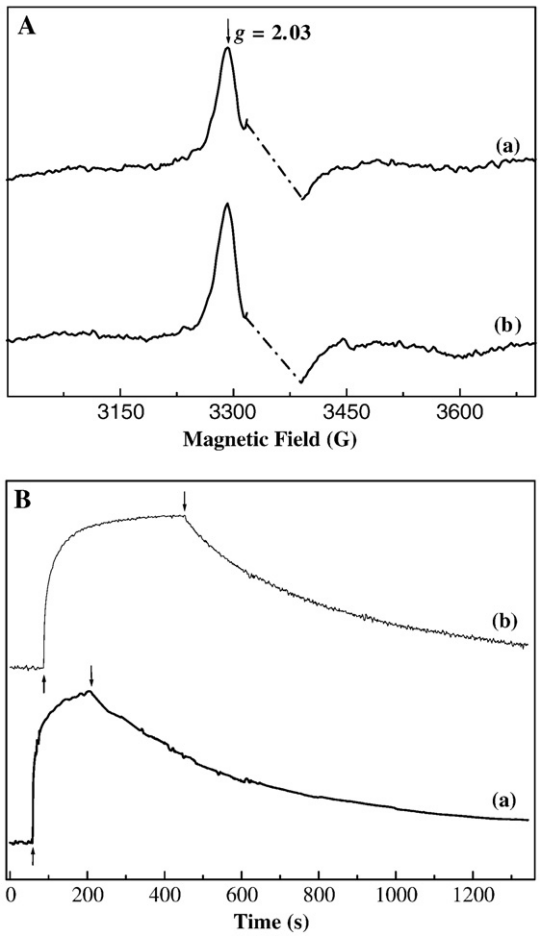


**Fig. 2.** (A). $S_1Tyr_Z$· EPR signal induced from PSII enriched membranes by visible light at 7 K. The spectrum is the difference spectrum obtained by subtracting the spectrum recorded before illumination from the spectrum recorded during illumination. (a) $K_3Fe(CN)_6$-treated sample (see text for detail); (b) untreated sample. For clarity, $Tyr_D$· signal in the middle of the spectrum was deleted. EPR conditions: Temperature, 7 K; Microwave power, 1 mW; Modulation amplitude, 18 G; Modulation frequency, 100 kHz. (B). Induction and decay kinetics of the $S_1Tyr_Z$· EPR signal from $K_3Fe(CN)_6$-treated sample (curve a) and untreated sample (curve b) monitored at 3295 G as indicated by the arrow in panel A. EPR conditions: Conversion time, 1311 ms; Time constant, 655 ms; Sweep time, 1342 s; other settings are the same as in panel A. The arrows in panel B indicate when the light was turned on (↑) and off (↓).

longer life-time for $S_1Tyr_Z$· if the non-heme iron is in the $Fe^{3+}$ state in the same reaction centers.

Fig. 2A shows the EPR spectra induced by visible light at 7 K in $K_3Fe(CN)_6$ treated and untreated samples. The $g$=2.03 EPR signal is similar to previous reports [41–43]. It has been demonstrated to be arisen from the magnetic interaction between $Tyr_Z$· and Mn-cluster in the $S_1$ state ($S_1Tyr_Z$·). The weak EPR signal around 3450 G ($g$=1.94) of spectrum b in Fig. 2A was originated from $Q_A^{-}$·$Fe^{2+}$[44], because this signal did not decay at 7 K during half an hour in the dark (data not shown), and it was not observed in the $K_3Fe(CN)_6$-treated sample (spectrum a in Fig. 2A). Thus it should not be correlated with the oxidation of $Tyr_Z$. Surprisingly, the yields of $Tyr_Z$· obtained in Fig. 2A are essentially the same in $K_3Fe(CN)_6$-treated and untreated samples. It was estimated that 40% of the reaction centers gave rise to the $S_1Tyr_Z$· EPR signal in untreated PSII sample [44]. Therefore, we deduce that a similar population of the reaction centers gives rise to the $S_1Tyr_Z$· EPR signal in $K_3Fe(CN)_6$-treated PSII sample as well. The decay kinetics of the $S_1Tyr_Z$· signal ($g$=2.03) from $K_3Fe(CN)_6$-treated and untreated samples are shown in Fig. 2B. Again, no obvious difference is observed for the decay kinetics of $Tyr_Z$· in both samples, with the half-decay time of the $S_1Tyr_Z$· signal of about 5 min. Similar results were obtained in PSII core complex isolated from *T. vulcanus* (data not shown, but see Fig. 5A). The yields and decay kinetics observed here were well reproducible among different preparations. It should be pointed out that the rise kinetics of $S_1Tyr_Z$· EPR signal is sensitive to the experiment conditions (e.g. concentration of Chl and the type of buffer, light intensity, etc.). The real half rise time for the formation of $S_1Tyr_Z$· was less than 10 ms as reported by Zhang, et al.[42,44], and it cannot be resolved in the continuous illumination experiment. Thus, the rise part in the trace recorded during illumination in Fig. 2B should not reflect the real properties of the induction kinetic of $S_1Tyr_Z$·.

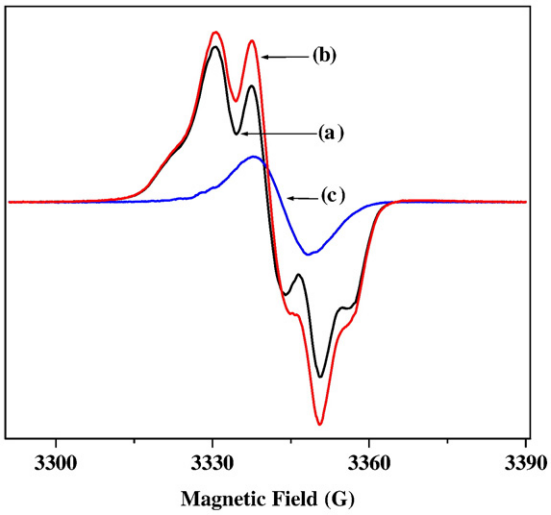


**Fig. 3.** EPR spectra at the $g$=2.00 radical region, recorded before visible light illumination (a) and during illumination (b) in 10 mM $K_3Fe(CN)_6$-treated PSII core complex from *T. vulcanus*. Spectrum (c) is the difference spectrum obtained by subtracting the spectrum (a) from (b). EPR condition: Microwave power, 1 μW; modulation amplitude, 4 G. Other conditions are the same as in Fig. 2A.

The similar yield of formation and decay kinetic of $S_1Tyr_Z$· in $K_3Fe(CN)_6$-treated and untreated sample as shown in Fig. 2 suggested that the charge pair formed was [$S_1Tyr_Z$·—$Q_A^{-}$·$Fe^{2+}$] in both $K_3Fe(CN)_6$-treated and untreated samples, and there was no sign of [$S_1Tyr_Z$·— $Q_AFe^{2+}$] charge pairs formed under these experimental conditions.

Fig. 3 shows the spectral changes at $g$=2.00 radical region recorded in $K_3Fe(CN)_6$-treated PSII core complex from *T. vulcanus* before and after visible light illumination. The difference spectrum after light

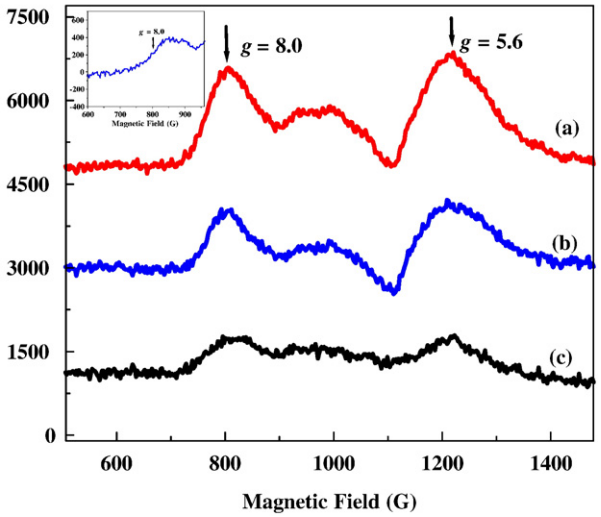


**Fig. 4.** EPR spectra at higher g value region, recorded before visible light illumination (a) and during illumination (b) in 10 mM $K_3Fe(CN)_6$-treated PSII core complex from *T. vulcanus*. spectrum (c) obtained by subtracting the spectrum (a) from (b). Insert is the spectrum recorded in untreated PSII core complex isolated from *T. vulcanus*, which was shown as the background of the spectra (a) and (b). EPR conditions are the same as in Fig. 2A.

illumination (curve c) shows a narrow radical EPR signal, which is about 10 G wide (peak to though) and is stable in the dark for several hours at cryogenic temperatures. The narrow radical EPR signal has been assigned to Car/$Chl_Z$ radicals [35,40]. Similar results were observed in untreated spinach PSII enriched membranes as well (data not shown, but see Ref. [44]).

Fig. 4 shows the EPR spectra at higher g value region obtained with PSII core complex from *T vulcanus*. Spectrum (a) and (b) were taken before and after illumination from $K_3Fe(CN)_6$-treated PSII sample. The observation of the $g$=8.0 EPR signal indicates the formation of the oxidized non-heme iron after the $K_3Fe(CN)_6$-treatment [50,53,54,56]. Upon illumination, the $g$=8.0 EPR signal was significantly decreased, indicating the reduction of $Fe^{3+}$ [50,53–56]. Spectrum (c) is the difference obtained by subtracting spectrum (b) from spectrum (a). It is important to note that the decrease is not completely recovered in several hours in the dark, which is similar to the stability of $Car^{+\cdot}/Chl_Z^{+\cdot}$ EPR signal as shown in Fig. 3 (c).

Fig. 5A shows the time-dependent spectra of $S_1Tyr_Z\cdot$ EPR signal ($g$=2.03) after illumination of the $K_3Fe(CN)_6$-treated PSII core complex isolated from *T. elongatus*. It is clear that the amplitude of $S_1Tyr_Z\cdot$ signal decreased rapidly in the dark. After 24 min, more than 90% of the $S_1Tyr_Z\cdot$ signal disappeared (see Fig. 5A, curve d). This result is consistent with the observation of the kinetic study of the $S_1Tyr_Z\cdot$ in Figs. 2B and 6 (see below). Fig. 5B shows the time-dependent spectra of reduction of $Fe^{3+}$ signal. The light induced decrease of the $g$=8.0 and 5.6 EPR signals, which is due to the reduction of $Fe^{3+}$, is shown as the negative peaks in spectrum a in Fig. 5B. It was found that the negative peak at $g$=8.0 position had no obvious change during 24 min in the dark (see spectra b, c and d), indicating that there was no obvious re-oxidation of $Fe^{2+}$ during this time. Thus, the reduced state of the non-heme iron is rather stable, which is significantly different from the fast decay of $S_1Tyr_Z\cdot$.

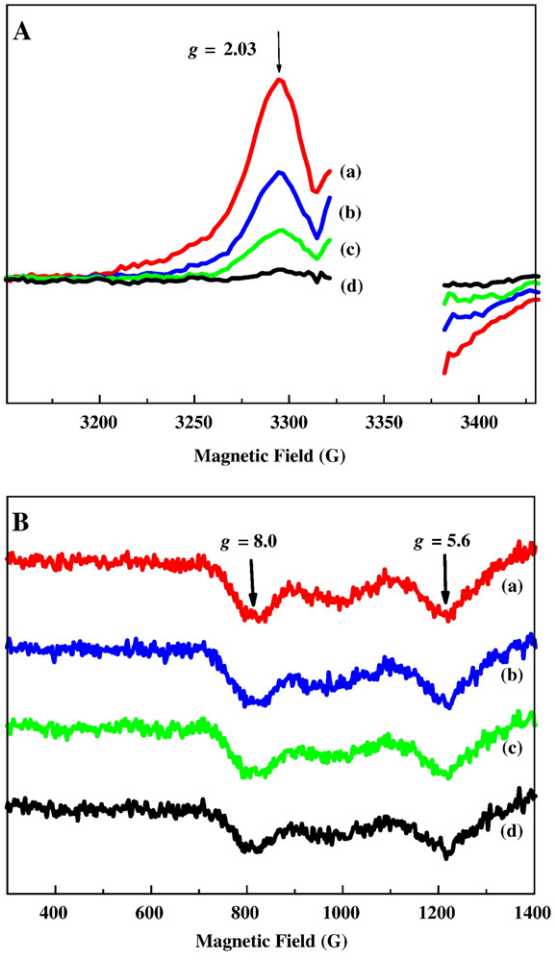


**Fig. 5.** Time-dependent spectra of $S_1Tyr_Z\cdot$ EPR signal (A) and the reduction of the $Fe^{3+}$ EPR signal (B) after light illumination on the $K_3Fe(CN)_6$-treated PSII core complex from *T. vulcanus*. The difference spectra in Fig. A are obtained from the spectra recorded at different times: (a) during illumination, (b) from 0 to 6 min after illumination, (c) from 6 to 12 min after illumination, and (d) from 18 to 24 min after illumination, minus the spectrum recorded 24 min after illumination at 7 K. The $g$=2.00 region corresponding to the $Tyr_D\cdot$ absorption is omitted. The difference spectra in Fig. B are obtained from the spectra recorded at the same different times as in Fig. A, minus the spectrum recorded before illumination at 7 K. EPR conditions are the same as in Fig. 2A.

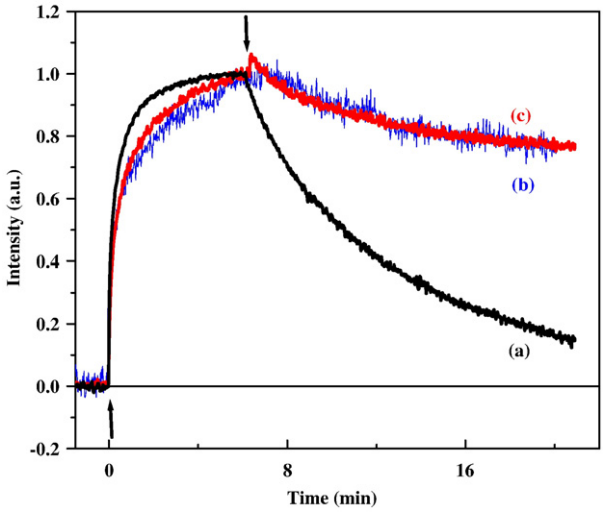


**Fig. 6.** Kinetic traces of the $g$=2.03 (curve a), $g$=8.0 (curve b) and $g$=2.00 EPR signals (curve c), recorded in 10 mM $K_3Fe(CN)_6$-treated PSII core complex from *T. vulcanus*, monitored at magnetic field of 3290 G (a), 800 G (b) and 3347 G (c), respectively. The microwave power is 1 mW (a), 1 mW (b) and 1 μW(c), respectively. The modulation amplitude is 18 G (a), 18 G (b), and 4 G (c), respectively. Other EPR conditions are the same as in Fig. 2A. For clarity, all three kinetic traces are normalized to positive 1 and superimposed. Arrows indicate when the illumination light was turned on (↑) and off (↓).

Fig. 6 shows the decay kinetics of $S_1Tyr_Z\cdot$ (curve a), $Car^{+\cdot}/Chl_Z^{+\cdot}$ (curve c) and oxidized non-heme iron ($Fe^{3+}$, curve b) in $K_3Fe(CN)_6$-treated PSII core complex from *T. vulcanus*. The rise and decay of $S_1Tyr_Z\cdot$ signal correspond to $Tyr_Z$ oxidation induced by visible light illumination and $Tyr_Z\cdot$ re-reduction in the dark, respectively. For the $Car^{+\cdot}/Chl_Z^{+\cdot}$ signal at $g$=2.00, the original kinetic trace was composed by an initial decrease followed by a recovery, indicating the oxidation of Car/$Chl_Z$ and re-reduction of $Car^{+\cdot}/Chl_Z^{+\cdot}$. Similarly, a decrease and recovery of the $g$=8.0 EPR signal reflect $Fe^{3+}$ reduction and $Fe^{2+}$ re-oxidation, respectively. For clarity, we normalized all three kinetic traces to positive 1, and superimposed them in Fig. 6. It is noted that the rise kinetics of $S_1Tyr_Z\cdot$, Car/$Chl_Z$ radical and reduction of $Fe^{3+}$ during illumination are sensitive to experimental conditions such as concentration of Chl, the type of buffer and light intensity, etc.; thus they could not be resolved by the present continuous illumination protocol. Dramatically different kinetics are observed between $S_1Tyr_Z\cdot$ and the $Car^{+\cdot}/Chl_Z^{+\cdot}$, $Fe^{2+}$ re-oxidation signals in the dark. A first-order exponential fit of the apparent decay part in Fig. 6 gave the time constant of 6 min for $S_1Tyr_Z\cdot$ and 6–7 min for $Car^{+\cdot}/Chl_Z^{+\cdot}$ and $Fe^{3+}$, respectively. The $S_1Tyr_Z\cdot$ EPR signal decays almost completely in the 20 min time window, and the 6 min of the time constant is consistent with the previous report [42,44]. However, only 20% of the total amplitudes of $Car^{+\cdot}/Chl_Z^{+\cdot}$ and $Fe^{3+}$ signals decay within the same time window. The $Car^{+\cdot}/Chl_Z^{+\cdot}$ EPR signal is known to live for several hours at liquid helium temperatures (see above and also ref. [42] and [44]). We observed that the decrease of the $g$=8.0 $Fe^{3+}$ EPR signal was not completely recovered after several hours in the dark (see Fig. 5 also),

similar to the stability of the $Car^{+\cdot}/Chl_Z^{+\cdot}$ signal. Therefore, the half-decay time for the $Car/Chl_Z$ radical and re-oxidation of $Fe^{2+}$ are obviously longer than half an hour, and their full decay kinetics could not be resolved by present data due to their long life-time at 7 K. Interestingly, the decay traces for $Car^{+\cdot}/Chl_Z^{+\cdot}$ and $Fe^{3+}$ signals are almost identical, and both decay slowly in the dark. Clearly, the recovery of $Fe^{3+}$ signal is related to the reduction of $Car^{+\cdot}/Chl_Z^{+\cdot}$ instead of $Tyr_Z^{\cdot}$, which indicates that the electron used for the reduction of $Fe^{3+}$ comes from $Car/Chl_Z$ but not $Tyr_Z$.

According to the close correlation between the reduction of $Fe^{3+}$ and $Car/Chl_Z$ oxidation observed here (Fig. 6), we were able to estimate the yield of the $g$=8.0 EPR signal in Fig. 4 (a) based on the amount of the $Car^{+\cdot}/Chl_Z^{+\cdot}$ formed. We have estimated the number of centers in which the $Car/Chl_Z$ radical is formed by comparing the $g$=2.00 signal (Fig. 3, curve c) with the signal from the stable $Tyr_D^{\cdot}$ (Fig. 3, curve a). The amount of the radical formed can be determined by comparing the double integration of the $Tyr_D\cdot$ absorption (Fig. 3, curve a) with the signal induced by illumination (Fig. 3, curve c). In this experiment, we found that the yield of $Car/Chl_Z$ oxidation is approximately 20±2%. It is noted that the quantification method used here has been widely used to quantify the $Car/Chl_Z$ radical in literatures (See ref. [42,44] for example). Since $Cyt_{b559}$ was fully oxidized in the $K_3Fe(CN)_6$-treated sample, it should not be involved in electron transfer any more. Thus, the proportion of reaction centers involved in forming the $Car/Chl_Z$ radical (Fig. 3, curve c) should be equal to the proportion of centers occurring on the reduction of $Fe^{3+}$ as shown in the curve c of Fig. 4. The total proportion of reaction centers involved in forming $Fe^{3+}$ in curve a of Fig. 4 can be estimated by comparing the amplitude of the $Fe^{3+}$ signal ($g$=8.0) formed after $K_3Fe(CN)_6$-treatment in the dark with that from the reduction of $Fe^{3+}$ (Fig. 4, curve c) after illumination at 7 K. This gives us approximately 50–60% of centers. Namely, the non-heme iron in 50–60% of the reaction centers is oxidized in our experiments. This value is consistent with previous reports [50,56], which indicates that the oxidation of non-heme iron only occurs in some fractions of the reaction centers. Considering the estimation for $Tyr_Z$ oxidation of 40% in the same experimental conditions, we rationale that there exist two types of reaction centers in intact PSII: one contains oxidizable $Fe^{2+}$; another one contains unoxidizable $Fe^{2+}$. The oxidation of the side-path electron donor occurs only in the fraction of reaction centers containing oxidizable non-heme iron; whereas $Tyr_Z$ oxidation takes place in the rest of reaction centers containing the unoxidizable $Fe^{2+}$. Therefore, $Tyr_Z$ oxidation is independent of the treatment of $K_3Fe(CN)_6$. In other words, oxidations of $Tyr_Z$ and $Car/Chl_Z$ occur separately in different reaction centers, and do not compete with each other in the same reaction center.

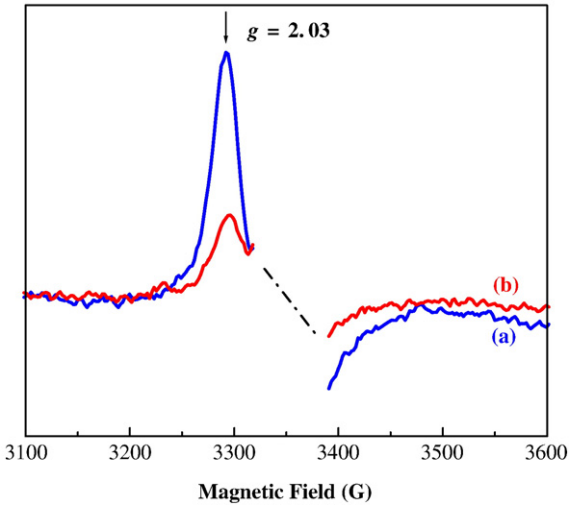


**Fig. 7.** Effect of PPBQ on the $S_1Tyr_Z\cdot$ signal induced by visible light at 7 K. The spectrum is the difference spectrum obtained by subtracting the spectrum recorded 30 min after illumination in the dark from the spectrum recorded during illumination on PSII enriched membranes containing 1 mM PPBQ (a) and 0 mM PPBQ (b), respectively. The middle range of the spectrum due to $Tyr_D\cdot$ signal was deleted for clarity. EPR conditions are the same as in Fig. 2A.

### 3.2. $Q_B$ effect

In recent studies of $Tyr_Z$ oxidation at cryogenic temperatures, either the physiological quinone (PQ) [44] or external quinone (such as PPBQ) [41–43,52] was present at the position of $Q_B$. It is interesting to verify if the presence of $Q_B$ is necessary for the electron transfer reactions in intact PSII at low temperature, especially, $Tyr_Z$ oxidation, although the electron transfer from $Q_A^{-\cdot}$ to $Q_B$ is known to be blocked [32,33]. $S_1Tyr_Z\cdot$ EPR signals induced by visible light in the presence (a) and absence (b) of 1 mM PPBQ in intact PSII at 7 K are shown in Fig. 7. The amplitude of the $S_1Tyr_Z\cdot$ EPR signal in the absence of PPBQ is decreased to 33% of that in the presence of PPBQ. On the other hand, the yield of $Car/Chl_Z$ oxidation was significantly increased in the absence of PPBQ (data not shown). Obviously, the presence of PPBQ significantly enhanced the yield of $Tyr_Z$ oxidation. One may argue that the electron transfer could occur between $Q_A$ and PPBQ at liquid helium temperatures. If so, we would expect that the decay kinetics of $S_1Tyr_Z\cdot$ was significantly different between the samples with and without PPBQ. However, we found that the half life-times of the $S_1Tyr_Z\cdot$ EPR signal in both cases were the same (about 5 min in the dark, data not shown). Therefore, the enhancement of $Tyr_Z$ oxidation observed should be not related to the occurrence of the electron transfer between $Q_A$ and PPBQ at low temperature.

## 4. Discussion

### 4.1. Relationship between the oxidation of $Tyr_Z$ and side-path electron donors

Our results show that the properties of the acceptor side have significant effect on the selectivity of electron transfer reactions in intact PSII at cryogenic temperatures. $Tyr_Z$ oxidation and side-path reaction probably occur separately in different PSII reaction centers at cryogenic temperatures, namely, $Tyr_Z$ oxidation occurs exclusively in the reaction centers containing unoxidizable non-heme iron; while $Car/Chl_Z$ oxidation takes place in reaction centers containing the oxidizable non-heme iron. In the following, we discuss two possibilities accounting for this observation. One is the electrostatic effect, and the other one is the structural factors.

In our experiments, although there are different electron donors to $P680^{+\cdot}$, $Q_A$ is the sole electron acceptor in the reaction center, because electron transfer from $Q_A$ to $Q_B$ is known to be completely blocked at cryogenic temperatures. There is no doubt that the more stable $Q_A^{-\cdot}$ would have higher ability to stabilize the charge separation state between $Q_A$ and $P_{680}^{+\cdot}$. Because the non-heme iron is known to interact with $Q_A$ through a H-bond directly [3,5], any change on $Fe^{2+}$ would be expected to significantly affect the stability of $Q_A^{-\cdot}$. The non-heme iron in high potential form should provide higher stabilization energy on $Q_A^{-\cdot}$ due to electrostatic effect than the low potential form does. Thus, the charge recombination between $Tyr_Z\cdot$ and $Q_A^{-\cdot}$ would be slower in reaction centers with high potential non-heme iron, which would contribute to increase the yield of the oxidation of $Tyr_Z$ by $P_{680}^{+\cdot}$. On the other hand, the observed PPBQ enhancement on $S_1Tyr_Z\cdot$ signal can also be explained by the electrostatic effect. It has been found that one proton is released from one residue upon the oxidation of the non-heme iron revealed by the pH-titration experiment [50]. The residue was suggested to be D1-His215 [57] or D1-His252 [58]. It is noted that both of these two residues can interact with $Q_B$ through H-bond [3,5]. Obviously, the presence of PPBQ at $Q_B$ position obstructs the release of

proton from these residues, as a result, the redox potential of the non-heme iron may be raised [50,58,59].

Besides the electrostatic effect, possible structural factors should be considered as well. Structural cooperation between the acceptor side and donor side has been suggested in inhibited PSII [60]. We anticipate that changes on the non-heme iron and $Q_B$ at the acceptor side may cause some changes on components at the donor side, e.g. $P_{680}$ and $Tyr_Z$, through a long distance mutual structural cooperation in intact PSII. It has been suggested that $Tyr_Z$ interacts with D1-His190 through a low-barrier hydrogen bond [27]. If one speculates that the strength of this hydrogen bond is weakened, for example, due to changes on non-heme iron, the oxidation of $Tyr_Z$ would become difficult at cryogenic temperatures. Accordingly, Car/$Chl_Z$ competes to donate electron to $P_{680^{+\cdot}}$. On the other hand, it has been found that the delocalization of the positive charge on $P_{680^{+\cdot}}$ after charge separation may be different depending on different PSII preparations [61]. If the structure change results in positive charge density on $P_{D2}$ Chla over $P_{D1}$ Chla of the special pair, one would expect that the oxidation of $Tyr_Z$ will become difficult as well.

### 4.2. Two types of the non-heme iron in intact PSII

Our experiments and previous reports [54,56] on oxidation of non-heme iron by $K_3Fe(CN)_6$-treatment indicate that only some fractions of reaction centers can be oxidized, and suggest that there probably exist two types of reaction centers in intact PSII. One contains unoxidizable $Fe^{2+}$, and the other one contains oxidizable $Fe^{2+}$. On the other hand, it is known that there are two types of $Cyt_{b559}$, the high potential form and low potential form in normal PSII preparations. The low potential form $Cyt_{b559}$ exists in an oxidized state; while the high potential $Cyt_{b559}$ is in a reduced state. Thus it is important to know if the two type reaction centers reported here are related to the redox state of $Cyt_{b559}$. In our experiment, we found that the yield and decay kinetic of $Tyr_Z$ oxidation was actually the same in both untreated and $K_3Fe(CN)_6$-treated samples (Fig. 2). It is well known that $Cyt_{b559}$ is fully oxidized after treatment of high concentration of $K_3Fe(CN)_6$ (10 mM in our experiments). Therefore, it is clear that the redox state of $Cyt_{b559}$ is not correlated with the two type reaction centers reported here.

Since oxidation of $Tyr_Z$ occurs in the reaction centers containing unoxidizable $Fe^{2+}$, and oxidation of Car/$Chl_Z$ occurs in the reaction centers containing oxidizable $Fe^{2+}$, the two types of reaction centers may be assigned as active and inactive PSII, respectively. Among all ligands of the non-heme iron, the non-protein ligand (bicarbonate/carbonate) is known to be sensitive to various treatments. For example, it can be replaced by small anions and molecules, e.g. formate, $CN^-$, $F^-$, NO, etc. [11,62–65]. Considering the sensitivity of the non-protein ligand; we suggest that the ligation of the non-protein ligand could be different in active and inactive PSII. FTIR studies [57,66] suggested that the non-protein ligand might act as a bidentate ligand of the non-heme iron. This binding mode was supported by recent X-ray [3,5] studies. However, it should be pointed out that all FTIR studies of non-heme iron were carried out in Mn-depleted, inactive PSII, whereas the hydrogen atom of bicarbonate cannot be identified based on the current X-ray structural data. Therefore, the coordination of the non-protein ligand to non-heme iron in active PSII is still unclear. Unambiguous answers to the different properties of non-heme iron described here require further experimental and theoretical investigations in the active PSII in the future.

Finally, It was suggested that $Fe^{3+}$ may function as an intermediate species for the electron transfer between $Q_A$ and $Q_B$ in bacteria reaction centers (see ref. [67–70]) and also in PSII [50,53,58]. Our results show that formation of $Fe^{3+}$ due to the oxidation of non-heme iron by $K_3Fe(CN)_6$ can only be observed in the inactive PSII reaction centers; while the non-heme iron is unoxidizable in the active PSII. Therefore, it is likely that the $Fe^{3+}$ state of the non-heme iron is not involved in normal turnover of $Q_B$ reduction based on our low temperature electron transfer studies. It would be interesting to investigate if the $Fe^{3+}$ is an intermediate of the electron transfer between $Q_A$ and $Q_B$ at physiological temperatures.

## 5. Conclusion

We observe that the properties of acceptor side significantly affect the types of electron transfer reactions occurred at the donor side in intact PSII at cryogenic temperatures. Our results indicate that there are two types of reaction centers in intact PSII. One contains unoxidizable non-heme iron, and the other one contains oxidizable non-heme iron. Oxidations of $Tyr_Z$ and side-path electron donors occur separately in these two types of reaction centers, and do not compete with each other in the same reaction center. In addition, our results show that the non-heme iron is different between active and inactive PSII. The oxidation of non-heme iron takes place only in the inactive PSII, which implies that the $Fe^{3+}$ state is probably not the intermediate species for the normal turnover of $Q_B$ reduction in active PSII. These findings provided not only new insights on the electron transfer processes at cryogenic temperatures, but also clues to understanding the function of the side-path electron donors and the non-heme iron in intact PSII.

## Acknowledgments

This research was supported by the National Natural Science Foundation of China (NNSFC) with No. 20403024, 30570423, and Grants-in-Aid for Scientific Research from the Ministry of Education, Culture, Sports, Science and Technology of Japan.

## References

[1] A. Zouni, H.T. Witt, J. Kern, P. Fromme, N. Krauβ, W. Saenger, P. Orth, Crystal structure of photosystem II from *Synechococcus elongatus* at 3.8 Å resolution, Nature 409 (2001) 739–743.
[2] N. Kamiya, J.R. Shen, Crystal structure of oxygen-evolving photosystem II from *Thermosynechococcus vulcanus* at 3.7 Å resolution, Proc. Natl. Acad. Sci. U. S. A. 100 (2003) 98–103.
[3] K.N. Ferreira, T.M. Iverson, K. Maghlaoui, J. Barber, S. Iwata, Architecture of the photosynthetic oxygen-evolving center, Science 303 (2004) 1831–1838.
[4] J. Kern, B. Loll, A. Zouni, W. Saenger, K.D. Irrgang, J. Biesiadka, Cyanobacterial Photosystem II at 3.2 Å resolution — the plastoquinone binding pockets, Photosyn. Res. 84 (2005) 153–159.
[5] B. Loll, J. Kern, W. Saenger, A. Zouni, J. Biesiadka, Towards complete cofactor arrangement in the 3.0 Å resolution structure of photosystem II, Nature 438 (2005) 1040–1044.
[6] A.R. Holzwarth, M.G. Müller, M. Reus, M. Nowaczyk, J. Sander, M. Rögner, Kinetics and mechanism of electron transfer in intact photosystem II and in the isolated reaction center: Pheophytin is the primary electron acceptor, Proc. Natl. Acad. Sci. U. S. A. 103 (2006) 6895–6900.
[7] G. Renger, A.R. Holzwarth, Primary electron transfer, in: T.J. Wydrzynski, K. Satoh (Eds.), Photosystem II: The Light-Driven Water: Plastoquinone Oxidoreductase, Springer, The Netherlands, 2005, pp. 139–175.
[8] B.A. Diner, F. Rappaport, Structure, dynamics, and energetics of the primary photochemistry of photosystem II of oxygenic photosynthesis, Ann. Rev. Plant Biol. 53 (2002) 551–580.
[9] N. Nelson, C.F. Yocum, Structure and function of photosystem I and II, Ann. Rev. Plant Biol. 57 (2006) 521–565.
[10] V. Petrouleas, A.R. Crofts, The iron–quinone acceptor complex, in: T.J. Wydrzynski, K. Satoh (Eds.), Photosystem II: The Light-Driven Water: Plastoquinone Oxidoreductase, Springer, The Netherlands, 2005, pp. 177–206.
[11] B.A. Diner, V. Petrouleas, J.J. Wendoloski, The iron–quinone electron-acceptor complex of photosystem II, Physiol. Plant. 81 (1991) 423–436.
[12] C. Goussias, A. Boussac, A.W. Rutherford, Photosystem II and photosynthetic oxidation of water: an overview, Phil. Trans. R. Soc. Lond. B 357 (2002) 1369–1381.
[13] G. Renger, P. Kühn, Reaction pattern and mechanism of light induced oxidative water splitting in photosynthesis, Biochim. Biophys. Acta 1767 (2007) 458–471.
[14] B.A. Diner, G.T. Babcock, Structure, dynamics, and energy conversion efficiency in photosystem II, in: D.R. Ort, C.F. Yocum (Eds.), Oxygenic Photosynthesis: The Light Reactions, Kluwer Academic Publisher, The Netherlands, 1996, pp. 213–247.
[15] R.J. Debus, The manganese and calcium-ions of photosynthetic oxygen evolution, Biochim. Biophys. Acta 1102 (1992) 269–352.
[16] W. Hillier, J. Messinger, Mechanism of photosynthetic oxygen production, in: T.J. Wydrzynski, K. Satoh (Eds.), Photosystem II: The Light-Driven Water: Plastoquinone Oxidoreductase, Springer, The Netherlands, 2005, pp. 567–608.

[17] H. Dau, M. Haumann, Eight steps preceding O–O bond formation in oxygenic photosynthesis—a basic reaction cycle of the Photosystem II manganese complex, Biochim. Biophys. Acta 1767 (2007) 472–483.
[18] B.A. Diner, R.D. Britt, The redox-active tyrosines $Y_Z$ and $Y_D$, in: T.J. Wydrzynski, K. Satoh (Eds.), Photosystem II: The Light-Driven Water: Plastoquinone Oxidoreductase, Springer, The Netherlands, 2005, pp. 207–233.
[19] R.J. Debus, Amino acid residues that modulate the properties of tyrosine YZ and the manganese cluster in the water oxidizing complex of photosystem II, Biochim. Biophys. Acta 1503 (2001) 164–186.
[20] B.A. Diner, Amino acid residues involved in the coordination and assembly of the manganese cluster of photosystem II. Proton-coupled electron transport of the redox-active tyrosines and its relationship to water oxidation, Biochim. Biophys. Acta 1503 (2001) 147–163.
[21] C.W. Hoganson, G.T. Babcock, A metalloradical mechanism for the generation of oxygen from water in photosynthesis, Science 277 (1997) 1953–1956.
[22] C. Tommos, G.T. Babcock, Oxygen production in nature: a light-driven metalloradical enzyme process, Acc. Chem. Res. 31 (1998) 18–25.
[23] J.S. Vrettos, J. Limburg, G.W. Brudvig, Mechanism of photosynthetic water oxidation: combining biophysical studies of photosystem II with inorganic model chemistry, Biochim. Biophys. Acta 1503 (2001) 229–245.
[24] M. Haumann, A. Mulkidjanian, W. Junge, Tyrosine-Z in oxygen-evolving photosystem II: a hydrogen-bonded tyrosinate, Biochemistry 38 (1999) 1258–1267.
[25] M. Haumann, W. Junge, Photosynthetic water oxidation: a simplex-scheme of its partial reactions, Biochim. Biophys. Acta 1411 (1999) 86–91.
[26] M.L. Gilchrist, J.A. Ball, D.W. Randall, R.D. Britt, Proximity of the manganese cluster of photosystem II to the redox-active tyrosine YZ, Proc. Natl. Acad. Sci. U. S. A. 92 (1995) 9545–9549.
[27] C. Zhang, Low-barrier hydrogen bond plays key role in active photosystem II — a new model for photosynthetic water oxidation, Biochim. Biophys. Acta 1767 (2007) 493–499.
[28] J.H.A. Nugent, R.J. Ball, M.C.W. Evans, Photosynthetic water oxidation: the role of tyrosine radicals, Biochim. Biophys. Acta 1655 (2004) 217–221.
[29] D.H. Stewart, G.W. Brudvig, Cytochrome *b*559 of photosystem II, Biochim. Biophys. Acta 1367 (1998) 63–87.
[30] P. Faller, C. Fufezan, A.W. Rutherford, Side-path electron donors: cytochrome *b*559, chlorophyll Z and β-carotene, in: T.J. Wydrzynski, K. Satoh (Eds.), Photosystem II: The Light-Driven Water: Plastoquinone Oxidoreductase, Springer, The Netherland, 2005, pp. 347–365.
[31] A. Telfer, What is β-carotene doing in photosystem II reaction center? Phil. Trans. R. Soc. Lond. B 357 (2002) 1431–1440.
[32] A. Garbers, F. Reifarth, J. Kurreck, G. Renger, F. Parak, Correlation between protein flexibility and electron transfer from $Q_A^-$ to $Q_B$ in PSII membrane fragments from spinach, Biochemistry 37 (1998) 11399–11404.
[33] C. Fufezan, C. Zhang, A. Krieger-Liszkay, A.W. Rutherford, Secondary quinone in photosystem II of *Thermosynechococcus elongatus*: semiquinone-iron EPR signals and temperature dependence of electron transfer, Biochemistry 44 (2005) 12780–12789.
[34] P. Mathis, A. Vermeglio, Chlorophyll radical cation in photosystem II of chloroplasts. Millisecond decay at low temperature, Biochim. Biophys. Acta 396 (1975) 371–381.
[35] J. Hanley, Y. Deligiannakis, A. Pascal, P. Faller, A.W. Rutherford, Carotenoid oxidation in photosystem II, Biochemistry 38 (1999) 8189–8195.
[36] P. Faller, T. Maly, A.W. Rutherford, F. MacMillan, Chlorophyll and carotenoid radicals in photosystem II studied by pulsed ENDOR, Biochemistry 40 (2001) 320–326.
[37] C.A. Tracewell, A. Cua, D.H. Stewart, D.F. Bocian, G.W. Brudvig, Characterization of carotenoid and chlorophyll photooxidation in photosystem II, Biochemistry (2001) 193–203.
[38] B. Hillmann, E. Schlodder, Electron transfer reactions in photosystem II core complexes from *Synechcoccus* at low temperature-difference spectrum of $P_{680}^+Q_A^-$/$P_{680}Q_A$ at 77 K, Biochim. Biophys. Acta 1231 (1995) 76–88.
[39] T. Noguchi, T. Mitsuka, Y. Inoue, Fourier-transform infrared spectrum of the radical cation of β-carotene photoinduced in photosystem II, FEBS Lett. 356 (1994) 179–182.
[40] L.K. Thompson, G.W. Brudvig, Cytochrome *b*-559 may function to protect photosystem II from photoinhibition, Biochemistry 27 (1988) 6653–6658.
[41] J.H.A. Nugent, I.P. Muhiuddin, M.C.W. Evans, Electron transfer from the water oxidizing complex at cryogenic temperatures: the S1 to S2 step, Biochemistry 41 (2002) 4117–4126.
[42] C. Zhang, S. Styring, Formation of split electron paramagnetic resonance signals in photosystem II suggests that tyrosinez can be photooxidized at 5 K in the S0 and S1 states of the oxygen-evolving complex, Biochemistry 42 (2003) 8066–8076.
[43] D. Koulougliotis, J.R. Shen, N. Ioannidis, V. Petrouleas, Near-IR irradiation of the S2 state of the water oxidizing complex of photosystem II at liquid helium temperatures produces the metalloradical intermediate attributed to $S_1Yz^{\cdot}$, Biochemistry 42 (2003) 3045–3053.
[44] C. Zhang, A. Boussac, A.W. Rutherford, Low-temperature electron transfer in photosystem II: a tyrosyl radical and semiquinone charge pair, Biochemistry 43 (2004) 13787–13795.
[45] R.J. Debus, K.A. Campbell, D.P. Pham, A.M.A. Hays, J.M. Peloquin, R.D. Britt, Influence of D1-Glu189 on the properties of YZ and the manganese cluster in photosystem 2, in: G. Garab (Ed.), Photosynthesis: Mechanisms and Effects, vol. 2, Kluwer Academic Publishers, Dordrecht, 1998, pp. 1375–1378.
[46] J. Clausen, W. Junge, H. Dau, M. Haumann, Photosynthetic water oxidation at high $O_2$ backpressure monitored by delayed chlorophyll fluorescence, Biochemistry 44 (2005) 12775–12779.
[47] G. Christen, R. Steffen, G. Renger, Delayed fluorescence emitted from light harvesting complex II and photosystem II of higher plants in the 100 ns-5 micros time domain, FEBS Lett. 475 (2000) 103–106.
[48] M.Y. Kultisheva, E.R. Lovyagina, A.M. Kuznetsov, M.K. Solntsev, B.K. Semin, I.I. Ivanov, Comparative study of effects of artificial electron donors on the $A_T$-band of photosystem II thermoluminescence, Biochemistry (Moscow) 66 (2001) 715–720.
[49] D.A. Berthold, G.T. Babcock, C.F. Yocum, A highly resolved, oxygen-evolving photosystem II preparation from spinach thylakoid membranes, FEBS Lett. 134 (1981) 231–234.
[50] V. Petrouleas, B.A. Diner, Light-induced oxidation of the acceptor-side Fe(II) of photosystem II by exogenous quinones acting through the $Q_B$ binding site. I. Quinone, kinetics and pH-dependence, Biochim. Biophys. Acta 893 (1987) 126–137.
[51] J.R. Shen, N. Kamiya, Crystallization and the crystal properties of the oxygen-evolving photosystem II from *Synechococcus vulcanus*, Biochemistry 39 (2000) 14739–14744.
[52] C. Zhang, Interaction between $tyrosine_Z$ and substrate water in active photosystem II, Biochim. Biophys. Acta 1757 (2006) 781–786.
[53] J.L. Zimmermann, A.W. Rutherford, Photoreduction-induced oxidation of $Fe^{2+}$ in the electron-acceptor complex of photosystem II, Biochim. Biophys. Acta 851 (1986) 416–423.
[54] B.A. Diner, V. Petrouleas, $Q_{400}$, the non-heme iron of the photosystem II iron-quinone complex. A spectroscopic probe of quinone and inhibitor binding to the reaction center, Biochim. Biophys. Acta 895 (1987) 107–125.
[55] J.H.A. Nugent, Photoreducible high spin iron electron paramagnetic resonance signals in dark-adapted photosystem II: are they oxidised non-haem iron formed from interaction of oxygen with PS II electron acceptors?, Biochim. Biophys. Acta 1504 (2001) 288–298.
[56] R. Aasa, L.E. Andréasson, S. Styring, T. Väinngård, The nature of the Fe(III) EPR signal from the acceptor-side iron in photosystem II, FEBS Lett. 243 (1989) 156–160.
[57] R. Hienerwadel, C. Berthomieu, Bicarbonate binding to the non-heme iron of photosystem II investigated by Fourier transform infrared spectroscopy and $^{13}$C-labeled bicarbonate, Biochemistry 34 (1995) 16288–16297.
[58] H. Ishikita, E.W. Knapp, Oxidation of the non-heme iron complex in photosystem II, Biochemistry 44 (2005) 14772–14783.
[59] A.W. Rutherford, A. Krieger-Liszkay, Herbicide-induced oxidative stress in photosystem II, Trends Biochem. Sci. 26 (2001) 648–653.
[60] G.N. Johnson, A.W. Rutherford, K. Krieger, A change in the midpoint potential of the quinone $Q_A$ in photosystem II associated with photoactivation of oxygen evolution, Biochim. Biophys. Acta 1229 (1995) 202–207.
[61] T. Okubo, T. Tomo, M. Sugiura, T. Noguchi, Perturbation of the structure of $P_{680}$ and the charge distribution on its radical cation in isolated reaction center complexes of photosystem II as revealed by fourier transform infrared spectroscopy, Biochemistry 46 (2007) 6459–6467.
[62] D. Koulougliotis, T. Kostopoulos, V. Petrouleas, B.A. Diner, Evidence for $CN^-$ binding at the PSII non-heme $Fe^{2+}$. Effects on the EPR signal for $Q_A^-Fe^{2+}$ and on $Q_A/Q_B$ electron transfer, Biochim. Biophys. Acta 1141 (1993) 275–282.
[63] P. Pospíšil, A. Arató, A. Krieger-Liszkay, A.W. Rutherford, Hydroxyl radical generation by photosystem II, Biochemistry 43 (2004) 6783–6792.
[64] C.H. Goussias, Y. Deligiannakis, Y. Sanakis, N. Ioannidis, V. Petrouleas, Probing subtle coordination changes in the iron-quinone complex of photosystem II during electron transfer, by the use of NO, Biochemistry 41 (2002) 15212–15223.
[65] Y. Deligiannakis, V. Petrouleas, B.A. Diner, Binding of carboxylate anions at the non-heme Fe(II) of PSII. I. Effects on the $Q_A^-Fe^{2+}$ and $Q_AFe^{3+}$ EPR spectra and the redox properties of iron, Biochim. Biophys. Acta. 1188 (1994) 260–270.
[66] C. Berthomieu, R. Hienerwadel, Iron coorination in photosystem II: interaction between bicarbonate and the $Q_B$ pocket studied by fourier transform infrared spectroscopy, Biochemistry 40 (2001) 4044–4052.
[67] A. Remy, K. Gerwert, Coupling of light-induced electron transfer to proton uptake in photosynthesis, Nat. Struct. Boil. 10 (2003) 637–644.
[68] S. Hermes, O. Bremm, F. Graczarek, V. Derrien, P. Liebisch, P. Loja, P. Sebban, K. Gerwert, M. Haumann, A time-resolved iron-specific X-ray absorption experiment yields no evidence for an $Fe^{2+}\rightarrow Fe^{3+}$ transition during $Q_A^-\rightarrow Q_B$ electron transfer in the photosynthetic reaction center, Biochemistry 45 (2006) 353–359.
[69] H. Ishikita, E.W. Knapp, Electrostatic role of the non-heme iron complex in bacterial photosynthetic reaction center, FEBS Lett. 580 (2006) 4567–4570.
[70] J. Breton, Steady-state FTIR spectra of the photoreduction of $Q_A$ and $Q_B$ in *Rhodobacter sphaeroides* reaction centers provide evidence against the presence of a proposed transient electron acceptor X between the two quinones, Biochemistry 46 (2007) 4459–4465.